Neuronal Migration Is Regulated by Endogenous RNAi and Chromatin-Binding Factor ZFP-1/AF10 in *Caenorhabditis elegans*

Lisa M. Kennedy and Alla Grishok[1]
Department of Biochemistry and Molecular Biophysics, Columbia University, New York, New York 10032

ABSTRACT Endogenous short RNAs and the conserved plant homeodomain (PHD) zinc-finger protein ZFP-1/AF10 regulate overlapping sets of genes in *Caenorhabditis elegans*, which suggests that they control common biological pathways. We have shown recently that the RNAi factor RDE-4 and ZFP-1 negatively modulate transcription of the insulin/PI3 signaling-dependent kinase PDK-1 to promote *C. elegans* fitness. Moreover, we have demonstrated that the insulin/IGF-1-PI3K-signaling pathway regulates the activity of the DAF-16/FOXO transcription factor in the hypodermis to nonautonomously promote the anterior migrations of the hermaphrodite-specific neurons (HSNs) during embryogenesis of *C. elegans*. In this study, we implicate the PHD-containing isoform of ZFP-1 and endogenous RNAi in the regulation of HSN migration. ZFP-1 affects HSN migration in part through its negative effect on *pdk-1* transcription and modulation of downstream DAF-16 activity. We also identify a novel role for ZFP-1 and RNAi pathway components, including RDE-4, in the regulation of HSN migration in parallel with DAF-16. Therefore, the coordinated activities of DAF-16, ZFP-1, and endogenous RNAi contribute to gene regulation during development to ensure proper neuronal positioning.

WITH the identification of endogenous short interfering RNAs (endo-siRNAs) in many organisms, including plants, fungi, flies, nematodes, and mammals (reviewed in Li and Liu 2011), has come the challenge of identifying their biological and physiological roles. *Caenorhabditis elegans* endo-siRNAs that are generated by RNA-dependent RNA polymerases (RdRP) on messenger RNA (mRNA) templates (Ruby *et al.* 2006; Aoki *et al.* 2007; Pak and Fire 2007) have been termed 22G-RNAs due to the fact that they preferentially begin with guanosine and are 22 nucleotides in length (Gu *et al.* 2009). There are two main classes of 22G-RNAs, which are designated according to their interacting Argonaute protein. The first class includes 22G-RNAs antisense to protein-coding genes, which are found in complex with the Argonaute CSR-1 (Chromosome Segregation and RNAi-deficient) (Claycomb *et al.* 2009; Gu *et al.* 2009). 22G-RNAs of the second class, which are present in complex with the WAGO family of Argonautes, are antisense to transposons, pseudogenes, cryptic loci, and some coding genes (Gu *et al.* 2009).

RDE-4 is a double-stranded RNA (dsRNA)-binding protein and a member of the Dicer complex required to initiate silencing in response to exogenous RNAi (Parrish and Fire 2001; Tabara *et al.* 2002) and for the production of some endo-siRNAs (Lee *et al.* 2006; Vasale *et al.* 2010). We have previously demonstrated that RDE-4 cooperates with the RNAi-promoting factor Zinc-Finger Protein 1 (ZFP-1) (Dudley *et al.* 2002; Grishok *et al.* 2005; Kim *et al.* 2005) in modulating insulin/IGF-1 signaling (IIS) through its negative effect on transcription of the conserved 3-phosphoinositide-dependent kinase-1 (*pdk-1*) gene (Mansisidor *et al.* 2011). The upregulation of *pdk-1* in *rde-4(ne299)* and *zfp-1(ok554)* mutants was shown to be responsible for the increased sensitivity to stress and shortened life span observed in these animals (Mansisidor *et al.* 2011). We have recently discovered a novel function of the IIS pathway in the hypodermis, which serves to nonautonomously regulate hermaphrodite-specific neuron (HSN) migration in a DAF-16-dependent manner (Kennedy *et al.* 2013). Therefore, we were intrigued by the possibility that RNAi may also contribute to the regulation of IIS during embryogenesis to influence neuronal migration. Indeed, here we describe a role for both RNAi

Copyright © 2014 by the Genetics Society of America
doi: 10.1534/genetics.114.162917
Manuscript received October 7, 2013; accepted for publication February 13, 2014; published Early Online February 20, 2014.
Supporting information is available online at http://www.genetics.org/lookup/suppl/doi:10.1534/genetics.114.162917/-/DC1.
[1]Corresponding author: Department of Biochemistry and Molecular Biophysics, Columbia University, College of Physicians and Surgeons, 701 W. 168th Street, HHSC Room 611, New York, NY 10032. E-mail: ag2691@columbia.edu

factors and the chromatin-binding protein ZFP-1 in the regulation of HSN migration.

ZFP-1 is a homolog of mammalian AF10 (Acute Lymphoblastic Leukemia 1-Fused gene from chromosome 10) and is best known for its role in leukemia caused by its fusion to the mixed lineage leukemia (MLL) gene, which creates the MLL-AF10 oncogene (Chaplin *et al.* 1995). However, the normal developmental roles of AF10 remain elusive; therefore, studying its homolog ZFP-1 in *C. elegans* may help advance our understanding of this protein. In fact, recently, the highly conserved N-terminal plant homeodomain (PHD) fingers of ZFP-1 were shown to be essential for *C. elegans* viability (Avgousti *et al.* 2013). The PHD-finger domain of ZFP-1 interacts with methylated lysine 4 of histone H3 (H3K4me3) and promotes the localization of the protein to the promoters of active genes (including *pdk-1*) enriched in H3K4me3 during embryogenesis (Avgousti *et al.* 2013). Moreover, ZFP-1 was recently shown to be required for the recruitment of DOT-1.1, a histone H3 lysine 79 methyltransferase, to the promoters of highly expressed genes throughout development and to function, along with DOT-1.1, in the negative modulation of their transcription in a negative feedback mechanism (Cecere *et al.* 2013).

Here, we demonstrate that the long isoform of ZFP-1, which contains the N-terminal PHD fingers, is required for HSN migration. Combining epistasis analysis with the examination of DAF-16 subcellular localization, we show that the upregulation of *pdk-1* in *zfp-1* loss-of-function mutants contributes to the observed HSN undermigration phenotype by limiting DAF-16 nuclear activity. Furthermore, we implicate a number of RNAi factors, including the dsRNA-binding protein RDE-4, the dicer-related helicase DRH-3, and the Argonaute CSR-1, in the regulation of HSN migration. However, these genes are likely to function in parallel to DAF-16. Our study expands the limited understanding of the normal developmental roles of both ZFP-1/AF10 and endogenous RNAi by highlighting their requirement in establishing proper neuronal positioning during development.

Materials and Methods

C. elegans strains

Strains were maintained at 20° using standard methods (Brenner 1974). Bristol N2 was the wild-type strain used. The following strains were provided by the Hobert lab: SK4013 *zdIs13* (*tph-1*::*gfp)*IV (Clark and Chiu 2003) and OH8482 *otIs225 (cat-4*::*gfp)*II; *him-8*IV. The following strain was provided by the Hengartner lab: *zfp-1(op481)*III. The following strains were provided by the Jose lab: AMJ217 *rde-4(ne301)*III; *jamEx52* (*Punc-54*::*rde-4*(+)&3′ UTR plus *Punc-54*::*gfp*&3′ UTR) and AMJ188 *rde-4(ne301)*III; *jamEx3* (*Pf25b3.3*::*rde-4*(+)&3′ UTR plus *Pf25b3.3*::*gfp*&3′ UTR). The following mutant and transgenic strains were obtained through the *Caenorhabditis* Genetics Center: LGI—CF1038 *daf-16(mu86)*, WM153 *C04F12.1(tm1637)*, WM206 *drh-3 (ne4253)*, WM30 *rde-3(ne298)*, NL2098 *rrf-1(pk1417)*, EL476 *rrf-2(ok210)*; LGII—TJ1052 *age-1(hx546)*, NL2099 *rrf-3 (pk1426)*; LGIII—RB774 *zfp-1(ok554)*, CB4681 nDf17/qC1 *dpy-19(e1259) glp-1(q339)*; LGIV—WM193 {*csr-1(tm892)*IV; *neIs20* [pie-1::3xFLAG::csr-1 + unc-119(+)]}; LGV—WM158 *ergo-1(tm1860)*, *rde-1(ne300)*; LGX—JT709 *pdk-1(sa709)*, VC446 *alg-1(gk214)*. Compound mutant strains and transgenes used are as follows: AGK82—*zfp-1(ok554)*III; *tph-1*::*gfp*IV, AGK153—*zfp-1(op481)*III; *tph-1*::*gfp*IV, AGK154—{*zfp-1 (ok554) unc-119(ed3)*III; *tph-1*::*gfp*IV; *armIs5* [ZFP-1::FLAG *unc-119*(+)]}, AGK133—{*zfp-1(ok554) unc-119(ed3)*III; *tph-1*::*gfp*IV; *armEx5* [ZFP-1::GFP *unc-119*(+)]}, AGK156—{*zfp-1 (ok554) unc-119(ed3)*III; *tph-1*::*gfp*IV; *armEx14* [PHD1-PHD2:: FLAG ZFP-1 short *unc-119*(+)]}, AGK211—{*zfp-1(ok554) unc-119(ed3)*III; *tph-1*::*gfp*IV; *armIs2* [*unc-119*(+)]}, AGK343—{*zfp-1(ok554)*III; *tph-1*::*gfp*IV; *armEx91* [*punc-86*::*zfp-1(long isoform)*::*gfp* pPD118.33 (*myo-2*::*gfp)*]} (line 1 in figure S2A of this paper), AGK335—{*zfp-1(ok554)*III; *tph-1*::*gfp*IV; *armEx85* [*punc-86*::*zfp-1(long isoform)*::*gfp* pPD118.33 (*myo-2*::*gfp)*]} (line 2 in figure S2A of this paper), AGK336—{*zfp-1(ok554)*III; *tph-1*::*gfp*IV; *armEx86* [*punc-86*::*zfp-1(long isoform)*::*gfp* pPD118.33 (*myo-2*::*gfp)*]} (line 3 in figure S2A of this paper), AGK339—{*zfp-1(ok554)*III; *tph-1*::*gfp*IV; *armEx89* [*punc-86*:: *zfp-1(long isoform)*::*gfp* pPD118.33 (*myo-2*::*gfp)*]} (line 4 in figure S2A of this paper), AGK580—*daf-16(mu86)*I; *tph-1*::*gfp*IV, AGK236: *pdk-1(sa709)*X; *tph-1*::*gfp*IV, AGK155: *zfp-1(ok554)* III; *pdk-1(sa709)*X; *tph-1*::*gfp*IV, AGK470: *age-1(hx546)*II; *tph-1*::*gfp*IV, AGK285: *age-1(hx546)*II; *zfp-1(ok554)*III; *tph-1*::*gfp*IV, AGK277: *daf-16(mu86)*I; *age-1(hx546)*II; *zfp-1(ok554)*III; *tph-1*::*gfp* IV, AGK98: *rde-4(ne299)*III; *tph-1*::*gfp*IV, AGK246—*rde-4 (ne299)*III; *pdk-1(sa709)*X; *tph-1*::*gfp*IV, AGK268—*age-1 (hx546)*II; *rde-4(ne299)*III; *tph-1*::*gfp*IV, AGK124—*alg-1 (gk214)*X; *tph-1*::*gfp*IV, AGK81—*C04F12.1(tm1637)*I; *tph-1*:: *gfp*IV, AGK208—{*csr-1(tm892)*IV; *tph-1*::gfpIV; *neIs20* [pie-1::3xFLAG::csr-1 + unc-119(+)]}, AGK654—*drh-3(ne4253)*I; *tph-1*::*gfp*IV, AGK146: *tph-1*::*gfp*IV; *ergo-1(tm1860)*V, AGK144—*nrde-3(gg066)*; *tph-1*::*gfp*IV, AGK218: *tph-1*::*gfp*IV; *rde-1(ne300)*V, AGK194: *rde-3(ne298)*I; *tph-1*::*gfp*IV, AGK123: *rrf-1(pk1417)*I; *tph-1*::*gfp*IV, AGK121: *rrf-2(ok210)*I; *tph-1*:: *gfp*IV, AGK145: *rrf-3(pk1426)*II; *tph-1*::*gfp*IV, AGK710—{*zfp-1 (ok554)*III; *tph-1*::*gfp*IV; *armEx257* [*pdpy-7*::*daf-16b*::*tagrfp* pPD118.33 (*myo-2*::*gfp)*]}, AGK711—{*tph-1*::*gfp*IV; *armEx257* [*pdpy-7*::*daf-16b*::*tagrfp* pPD118.33 (*myo-2*::*gfp)*]}, AGK724—{*pdk-1(sa709)*X; *armEx257* [*pdpy-7*::*daf-16b*::*tagrfp* pPD118.33 (*myo-2*::*gfp)*]}, AGK725—{*zfp-1(ok554)*III; *pdk-1(sa709)*X; *armEx257* [*pdpy-7*::*daf-16b*::*tagrfp* pPD118.33 (*myo-2*::*gfp)*]}, AGK 721—{*rde-4(ne299)*III; *tph-1*::*gfp*IV; *armEx257* [*pdpy-7*::*daf-16b*::*tagrfp* pPD118.33 (*myo-2*::*gfp)*]}, AGK688—{*rde-4(ne299)*III; *tph-1*::*gfp*IV; *armEx273* [*pdpy-7*::*rde-4*:: *tagrfp* pPD118.33 (*myo-2*::*gfp)*]} (line 1 in figure 5B of this paper), AGK689—{*rde-4(ne299)*III; *tph-1*::*gfp*IV; *armEx274* [*pdpy-7*::*rde-4*::*tagrfp* pPD118.33 (*myo-2*::*gfp)*]} (line 2 in figure 5B of this paper), AGK690—{*rde-4(ne299)*III; *tph-1*::*gfp*IV; *armEx275* [*pdpy-7*::*rde-4*::*tagrfp* pPD118.33 (*myo-2*::*gfp)*]} (line 3 in figure 5B of this paper).

Molecular biology and transgenic lines

Standard molecular biology techniques were used to construct transgenes. Germline transformation was performed by direct injection of various plasmid DNAs into the gonads of adult wild-type animals as described (Mello *et al.* 1991). A *zfp-1*(long isoform) complementary DNA (cDNA) was obtained by PCR with N2 cDNA as a template with the forward primer containing the *Bal*I site 5′- ATGAAGAAGTGGC CAATGAAGGAGATGGTAGGTGGATGC-3′ and the reverse primer containing the *Age*I site 5′-CAAGTTATTGGTTACC GGTCCTTTTCCATTCGGAGTTGCAGATG-3.′ A 5.1-kb fragment upstream of the *unc-86* transcriptional start site was isolated by PCR from genomic DNA with the forward primer containing the *Sph*I site 5′-CGTGACACTGCATGCTTCAA AAACTGTCAACTAACAAGAT-3′ and the reverse primer containing the *Sal*I site 5′-CGGATGCGGTTGTCGACTCATTCA ATTTCACTTTTTCATTCG-3.′ The *zfp-1* cDNA and the *unc-86* promoter were subcloned into the Fire Kit GFP vector pPD95.75. The resulting *punc86*::*zfp-1*::*gfp* transgene was injected at 0.5 ng/μl with the co-injection marker pPD118.33 (*myo-2*::*gfp*) at 4 ng/μl. The *rde-4* cDNA was obtained by PCR with N2 cDNA as a template with the forward primer containing the *Bam*HI site 5′-TCACGTG GATCCATGGATTTAACCAAACTAACGTTTG-3′ and the reverse primer containing the *Kpn*I site 5′-TACTCAGGTACCCCAT CAAATCATAGGTGTTGA-3′. The *dpy*-7 (Gilleard *et al.* 1997) promoter was obtained by PCR with N2 genomic DNA as a template. The *dpy-7* promoter was amplified with the forward primer containing the *Sph*I site 5′-GTTATTGCATGCTCCACGATT TCTCGCAACACATCCC-3′ and the reverse primer containing the *Sal*I site 5′-GCGTCGGTCGACAAAGAACAGGGTGTGAT AAATGAAT-3.′ DNA was inserted into a modified Fire Kit vector pPD95.75, in which we replaced the GFP with a TAGRFP sequence using the *Kpn*I/*Eco*RI sites. *Pdpy-7*::*rde-4*::*tagrfp* was generated by inserting a *Sph*I/*Sal*I *dpy-7* fragment and *Bam*HI/*Kpn*I *rde-4* cDNA fragment into our modified pPD95.75 vector. The resulting *pdpy-7*::*rde-4*::*tagrfp* transgene was injected at 2.5 ng/μl with the co-injection marker pPD118.33 (*myo-2*::*gfp*) at 2.5 ng/μl. Tissue-specific GFP or TagRFP expression was confirmed using Nomarski and fluorescence microscopy.

Visualization of the HSN neurons

The HSN neurons were detected by staining adult hermaphrodites with rabbit anti-serotonin (Sigma) as previously described (Garriga *et al.* 1993) or by using the *zdIs13[tph-1*::*gfp]* or *otIs225[cat-4*::*gfp]* transcriptional reporters.

Microscopy and quantification

Live animals or embryos were mounted on 2% agarose pads and immobilized with 25 mM sodium azide (Sigma). Worms were examined using a Zeiss AxioImager Z1. All phenotypes were scored as the percentage of animals with at least one undermigrated HSN, and results are presented as stacked bar graphs in Figure 1, Figure 2, Figure 4, and Figure 5 to represent the proportion of HSNs in positions along the anterior–posterior (A–P) body axis in these animals. When one or both HSN cell bodies were located posterior to their normal position near the vulva in adult animals, the animal was scored as a mutant. The colored stacks within each column on the graphs presented in Figure 1, Figure 2, Figure 4, and Figure 5 represent the severity of migration of HSNs along the A–P axis within *only* those animals containing at least one undermigrated HSN. Thus, since there are two HSNs within each animal and not every HSN is undermigrated, a colored region could represent a HSN that remains unaffected in the animal, *i.e.*, the pink color in the graphs, while the other HSN within the same animal is undermigrated (one HSN must be affected for an animal to be included in the graph) and therefore represented by the reddish/purple, green, or blue color. Statistical significance was calculated using the *z*-test.

RNA extraction and RT-PCR

RNA extraction and reverse transcriptase PCR (RT-PCR) was carried out as described previously (Mansisidor *et al.* 2011). The following primers were used to detect the *pdk-1* transcript: 5′-CCTACAGCCAGGTATTCCG-3′ (forward) and 5′-GATCACGAAATAAATTCTAGCCTGG-3′ (reverse).

Results

C. elegans ZFP-1/AF10 regulates the migration of the HSNs

In our recent study (Kennedy *et al.* 2013), we showed that insulin/IGF-1-PI3K signaling modulates the activity of the DAF-16/FOXO transcription factor in the hypodermis to nonautonomously regulate the anterior migrations of the two bilaterally symmetric HSNs during embryogenesis of *C. elegans*. With the discovery that ZFP-1 negatively regulates *pdk-1*, a component of the IIS pathway, via direct repression of *pdk-1* transcription (Mansisidor *et al.* 2011), we were prompted to investigate the connection between ZFP-1 and IIS during HSN migration. We found that the *zfp-1 (ok554)* loss-of-function mutant (Cui *et al.* 2006; Avgousti *et al.* 2013; Cecere *et al.* 2013) and the *zfp-1(op481)* mutant (Gysi *et al.* 2013)—both of which lead to the generation of mRNAs that contain premature stop codons after the PHD fingers—display HSN undermigration defects (Figure 1, A–C). We used a tryptophan hydroxylase GFP reporter (*tph-1*::*gfp*) that marks the HSNs in adult animals for scoring the migration phenotype.

The *zfp-1(op481)* allele was originally isolated in a mutagenesis screen performed to identify genetic enhancers of a null mutation in the heparan sulfate proteoglycan core protein SDN-1, which is involved in D-type motor axon guidance (Gysi *et al.* 2013). Moreover, the *op481* allele was shown to exhibit an identical axon guidance phenotype as the *ok554* allele of *zfp-1* (Gysi *et al.* 2013). Surprisingly, however, the axon guidance phenotype in the *zfp-1(ok554)*; *sdn-1(zh20)* double mutant was dependent upon the presence

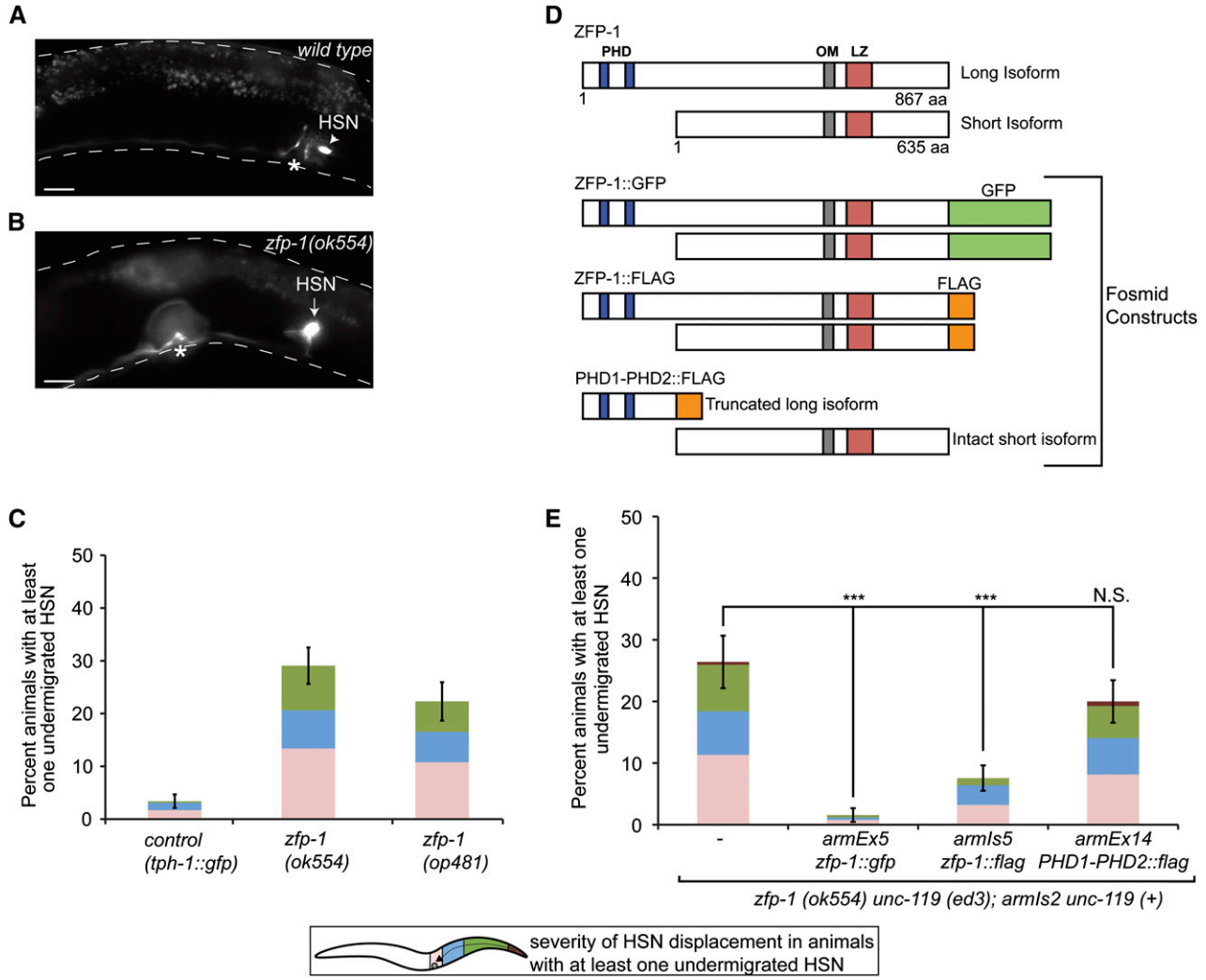

Figure 1 HSN undermigration defects in *zfp-1* mutants. (A) Epifluorescent images of the HSN in adults of wild-type (A) and *zfp-1(ok554)* mutant animals (B), visualized with a tryptophan hydroxylase GFP reporter (*tph-1*::*gfp*). Images are oriented with the posterior of the animal to the right. Asterisks indicate the vulva and the arrowhead in A denotes the position of properly migrated HSN(s). The arrow in B illustrates a HSN that has failed to migrate the full distance in the *zfp-1(ok554)* mutant animal. Bars, 20 μm. (C) Quantification of the percentage of animals with an undermigrated HSN from a minimum of two pooled independent experiments per strain in control *tph-1*::*gfp* (n = 177) *vs. zfp-1(ok554)* (n = 172) and *zfp-1(op481)* (n = 130) mutants. (D) The long isoform of ZFP-1 (867 aa) has two predicted PHD zinc fingers in the N terminus and an octapeptide motif and leucine zipper in the C terminus. The short isoform of ZFP-1 (635 aa) lacks the PHD fingers but retains the OM-LZ motifs. *zfp-1* fosmid constructs used to rescue the HSN undermigration defects present in the *zfp-1(ok554)* mutant are illustrated below the ZFP-1 proteins. Expression data for these ZFP-1 transgenes can be found in Avgousti *et al.* (2013). (E) Two different ZFP-1 fosmid constructs rescue the HSN undermigration defects in the *zfp-1(ok554)* mutants. The ZFP-1 fosmid construct expressing only an intact short isoform did not rescue the HSN undermigration defects present in the *zfp-1* mutant. Quantification of the percentage of animals with an undermigrated HSN from a minimum of two pooled independent experiments per strain in the (−) control *armIs2 Unc-119 (+)*; *zfp-1(ok554) unc-119 (ed3)* (n = 106) *vs.* the addition of the *armEx5 zfp-1*::*gfp* (n = 128), *armIs5 zfp-1*::*flag* (n = 172) or *armEx14 PHD1-PHD2*::*flag* (n = 135) fosmids into the (−) control background. HSNs were visualized with a *tph-1*::*gfp* reporter. The stacked bars show information about the position of all HSNs in the affected worms (see the description below). Worm schematic legend (located at the bottom center of the figure): Stacked bars represent the proportion of HSNs at different positions along the A–P body axis within only those animals containing at least one undermigrated HSN. Thus, since there are two HSNs within each animal and not every HSN is affected, one region (light pink) represents the wild-type HSN that remains unaffected in animals containing a second undermigrated HSN, which is represented by either the reddish/purple, green, or blue region. ***$P < 0.001$, N.S., not significant (z-test). For all figures, error bars represent standard error of the proportion (SEP) for the entire stacked column.

of the integrated transgene used to visualize the axon guidance defects (Gysi *et al.* 2013). Therefore, to exclude the possibility that the *tph-1*::*gfp* transgene was enhancing or causing the *zfp-1* mutant undermigration phenotype, we stained wild-type worms and *zfp-1* mutant worms with an anti-serotonin antibody (Garriga *et al.* 1993). The extent of HSN undermigration was similar in stained and transgenic worms, thereby ruling out the above possibility (Supporting Information, Figure S1, A–C). These results also suggest that ZFP-1 specifically affects the process of HSN migration, rather than cell fate, since all undermigrated HSNs showed expression of the neurotransmitter serotonin, a late step in

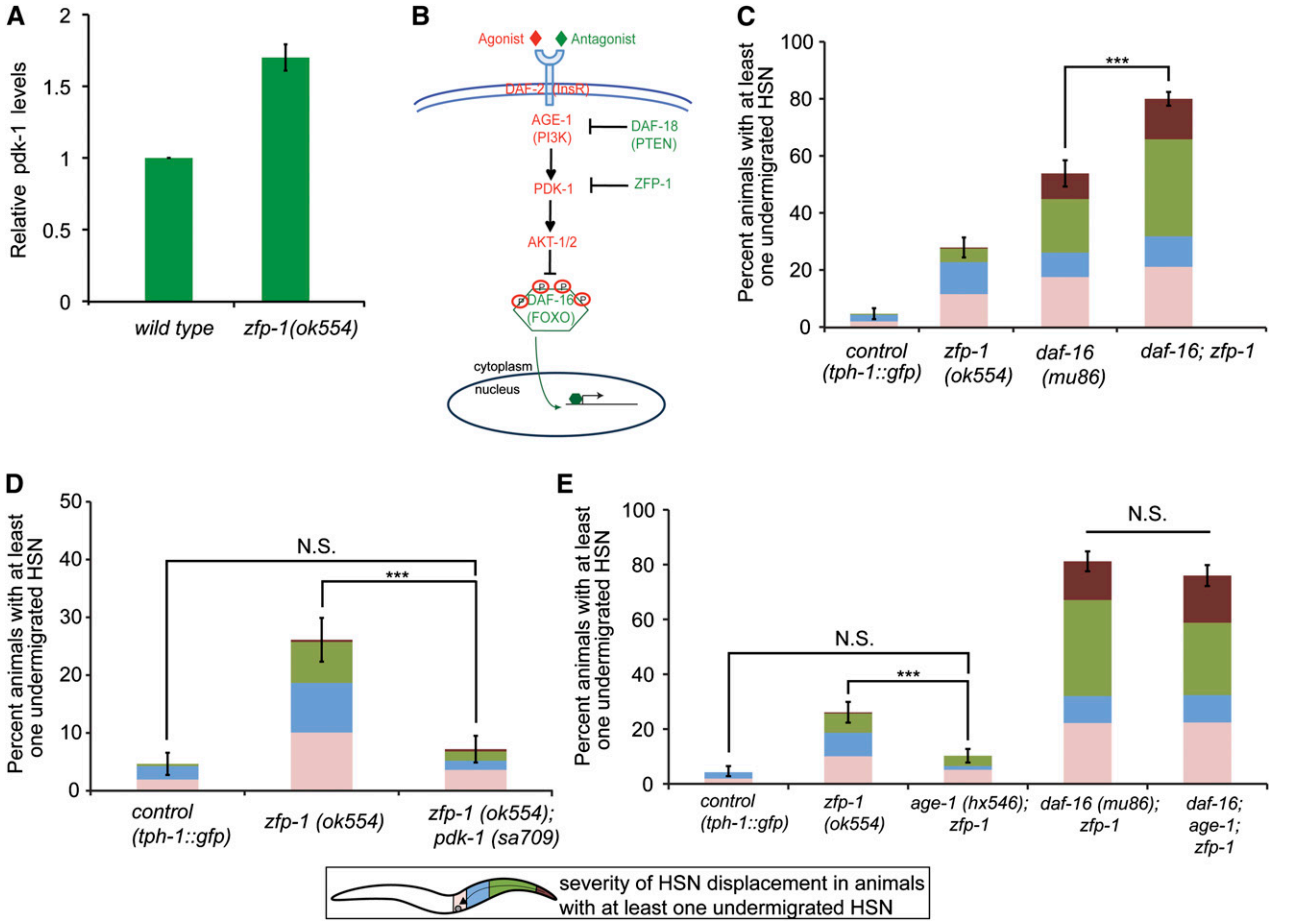

Figure 2 ZFP-1 functions through DAF-16 and in parallel to DAF-16 to regulate HSN migration. (A) Relative *pdk-1* mRNA expression in mixed embryos. mRNA expression of *pdk-1* in *zfp-1(ok554)* and wild-type worms was measured by RT-quantitative PCR and normalized to wild type. Actin (*act-3*) was used as an internal control. Results of two biological replicas are shown; error bars represent standard deviation. (B) Schematic of the IIS pathway affected by ZFP-1. When pathway components in red are active, DAF-16 is phosphorylated and inactive due to its retention in the cytoplasm. When pathway components in green are active, DAF-16 is no longer phosphorylated and can translocate into the nucleus to regulate its target genes. (C) The *zfp-1(ok554)* mutant enhances the *daf-16(mu86)* null mutant phenotype. Quantification of the percentage of animals with an undermigrated HSN from at least two pooled independent experiments per strain in control *tph-1*::*gfp* (n = 129) *vs. zfp-1(ok554)* (n = 165), *daf-16(mu86)* (n = 117), and *daf-16(mu86); zfp-1(ok554)* (n = 275) mutant animals. (D) A *pdk-1* loss-of-function mutant suppresses the HSN undermigration defects in *zfp-1* mutant animals. Quantification of the percentage of animals with an undermigrated HSN from two pooled independent experiments per strain in control *tph-1*::*gfp* (n = 129), *zfp-1(ok554)* (n = 134), and *zfp-1(ok554); pdk-1(sa709)* (n = 125) mutant animals. Note that *pdk-1(sa709)* animals do not exhibit HSN migration defects at 20 °C (not shown). (E) An *age-1(hx546)* loss-of-function mutant suppresses the HSN undermigration defects in *zfp-1* mutant animals in a DAF-16-dependent manner. Quantification of the percentage of animals with an undermigrated HSN from two pooled independent experiments per strain in control *tph-1*::*gfp* (n = 129) *vs. zfp-1(ok554)* (n = 134), *age-1(hx546); zfp-1(ok554)* (n = 146), and *daf-16(mu86); age-1(hx546); zfp-1(ok554)* (n = 125). Note that *age-1(hx546)* animals do not exhibit HSN migration defects at 20 °C (not shown). HSNs were visualized with a *tph-1*::*gfp* reporter. See Figure 1 for detailed description of worm schematic legend. ***P <0.001, N.S., not significant (z-test). Error bars represent SEP.

HSN maturation (Desai *et al.* 1988). Therefore, the phenotype of the *zfp-1* loss-of-function mutant is similar to the HSN defects that we observed in *daf-16* null mutants (Kennedy *et al.* 2013).

Long isoform of ZFP-1 is required for HSN migration

There are two isoforms of the ZFP-1 protein (Figure 1D): a long isoform that contains two PHD fingers, an octapeptide motif (OM) and a leucine zipper motif (LZ), and a shorter isoform that lacks the PHD fingers but retains the OM and LZ (Avgousti *et al.* 2013). The OM-LZ motifs present in both the long and the short isoforms have been shown to be required for MLL-AF10-mediated oncogenesis (DiMartino *et al.* 2002), whereas the PHD fingers present in the long isoform of ZFP-1 have recently been shown to be required for early development of *C. elegans* independent of the OM-LZ motifs (Avgousti *et al.* 2013). Moreover, it was demonstrated that the long isoform of ZFP-1 is preferentially expressed in the germline and embryos and that the short isoform is highly expressed at larval stages (Avgousti *et al.* 2013). Also, there is evidence that the long isoform of ZFP-1 binds to the *pdk-1* promoter during embryogenesis, when

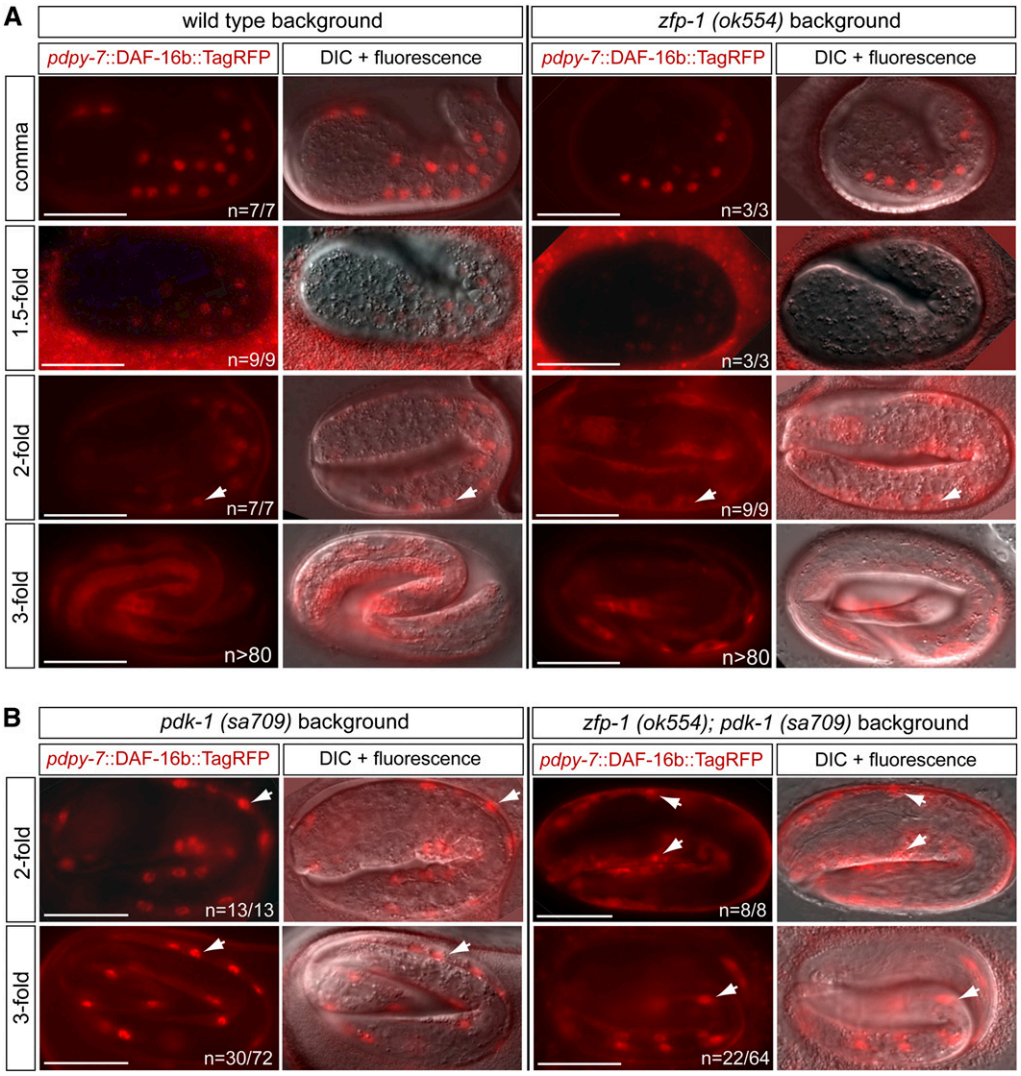

Figure 3 Mislocalization of hypodermally expressed DAF-16 in the *zfp-1(ok554)* mutant is partially restored by loss of *pdk-1*. (A) In wild-type animals, DAF-16b::TagRFP expressed from a hypodermal promoter is localized to the hypodermal nuclei during the comma, 1.5-, and 2-fold embryonic stages when HSN migration is occurring and is mostly cytoplasmic or perinuclear during the 3-fold stage (left panels). In the *zfp-1(ok554)* mutant, DAF-16b::TagRFP fails to persist in the nuclei during the 2-fold stage when HSN migration is still occurring (right panels). Arrows in the 2-fold panels point to hypodermal nuclei to illustrate that DAF-16b::TagRFP is nuclearly localized at this stage in wild-type embryos but not in *zfp-1 (ok554)* mutant embryos. (B) In the *pdk-1(sa709)* loss-of-function mutant, DAF-16b::TagRFP persists in the hypodermal nuclei from the 2-fold stage into the 3-fold stage in 30 of 72 embryos (left panels). The *pdk-1(sa709)* mutation partially suppresses the absence of DAF-16 nuclear location in *zfp-1(ok554)* mutant embryos during the 2-fold stage (right panels). Arrows in the 2-fold panels point to hypodermal nuclei to illustrate that DAF-16b::TagRFP is nuclearly localized in the *pdk-1(sa709)* mutant embryos and shows significant nuclear localization in the *zfp-1(ok554); pdk-1(sa709)* mutant embryos. Arrows in the 3-fold panels highlight examples of hypodermal nuclei in embryos in which DAF-16b::TagRFP persists after HSN migration has ended. Bars, 20 μm.

HSN migration takes place (Avgousti *et al.* 2013). Therefore, we sought to determine if the long isoform of ZFP-1 was required for HSN migration.

First, we made use of two different *zfp-1* fosmid constructs that express recombinant ZFP-1 protein isoforms tagged with either GFP or FLAG at the C-terminal portions of the proteins (Mansisidor *et al.* 2011) (Figure 1D) to rescue the *zfp-1(ok554)* HSN undermigration phenotype. These constructs contain all the regulatory sequences present at the *zfp-1* locus and recapitulate endogenous patterns of expression of ZFP-1 isoforms (Avgousti *et al.* 2013). We found that both fosmid constructs significantly rescued the HSN undermigration defects present in the *zfp-1(ok554)* mutant (Figure 1E). Next, to clarify which isoform(s) were required for rescue, we made use of another *zfp-1* fosmid that introduces a FLAG tag downstream of the PHD fingers followed by a stop codon, thereby leaving only the larva-enriched short isoform intact (Avgousti *et al.* 2013) (Figure 1D). In contrast to the fosmids that express both isoforms, this construct was unable to rescue the HSN undermigration defects present in the *zfp-1* mutant (Figure 1E). Moreover, overexpressing the N-terminal fragment of the ZFP-1 long isoform (PHD1-PHD2::FLAG), which is identical to the truncated fragment retained in the *zfp-1(ok554)* mutant (Figure 1D) (Avgousti *et al.* 2013), in the *zfp-1(ok554)* mutant background does not affect the penetrance of the HSN undermigration phenotype (Figure 1E). This result indicates that the residual fragment expressed in the *zfp-1(ok554)* mutant does not have neomorphic properties responsible for the HSN migration phenotype observed in the *zfp-1(ok554)* mutant because increased dosage of the fragment does not lead to increased severity of the phenotype. On the contrary,

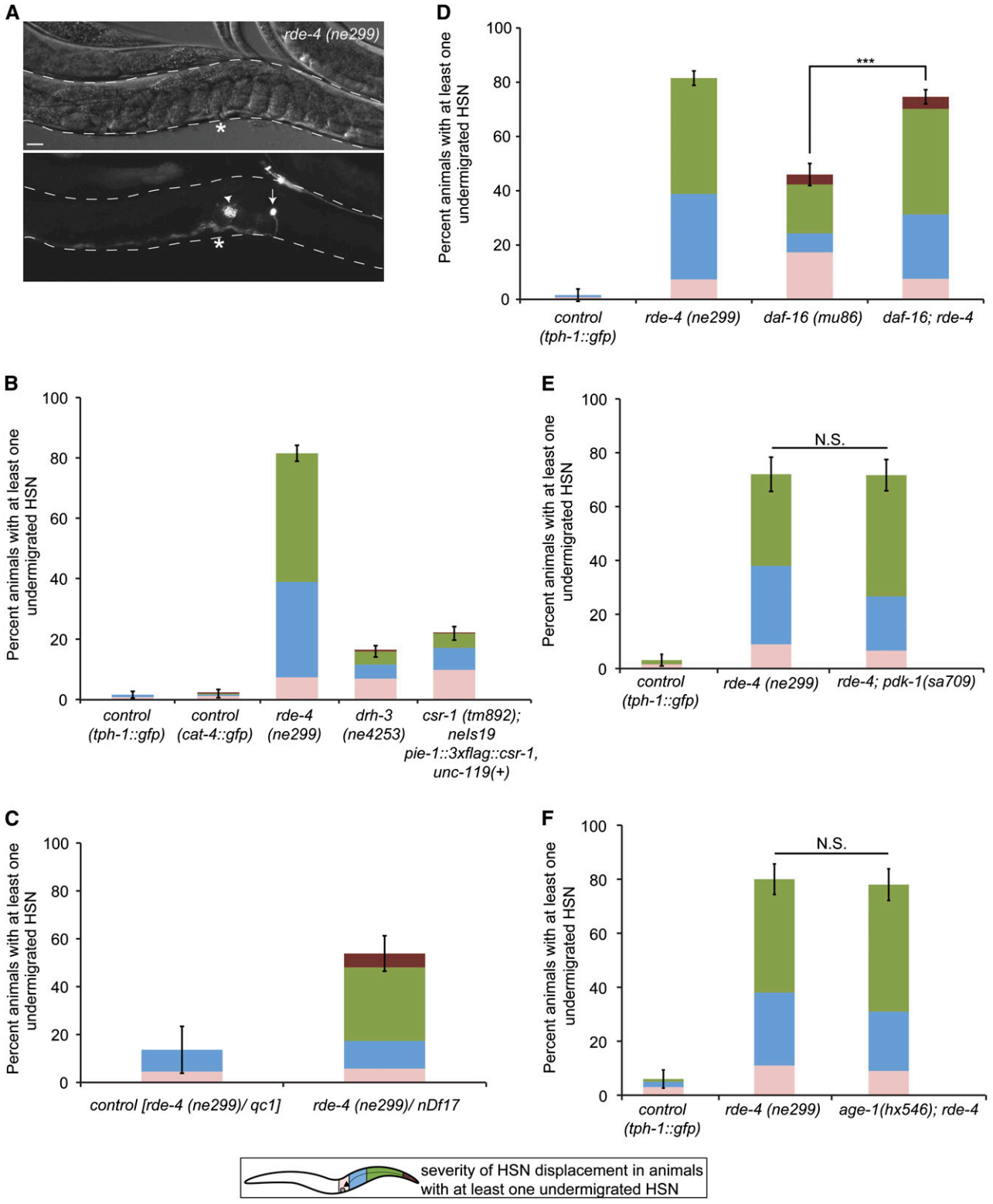

Figure 4 RNAi pathway genes *rde-4*, *drh-3*, and *csr-1* affect HSN migration. (A) Differential interference contrast image of adult hermaphrodite (top) and corresponding epifluorescent image of the HSN (bottom) in an adult *rde-4(ne299)* mutant animal. HSNs are visualized with a tryptophan hydroxylase GFP reporter (*tph-1*::*gfp)*. Image is oriented with the posterior of the animal to the right. Asterisk indicates the vulva and the arrowhead denotes the position of a properly migrated HSN. The arrow illustrates a HSN that has failed to migrate the full distance from its birthplace in the tail. (B) Quantification of the percentage of animals with an undermigrated HSN from a minimum of three pooled independent experiments per strain in *tph-1*::*gfp* (n = 127) and *cat-4*::*gfp* (n = 127) controls *vs. rde-4(ne299)* (n = 211), *drh-3(ne4253)* (n = 376), and the partially rescued *csr-1(tm982)* (n = 342) mutant animals. Note that the *cat-4*::*gfp* reporter was used to visualize the HSNs in the partially rescued *csr-1(tm892)* strain. (C) Placing *rde-4(ne299)*

previously reported data demonstrate that reducing the dosage of the PHD-finger domain is lethal (Avgousti *et al.* 2013). Importantly, it was also previously shown that the lethality of animals containing one copy of the *zfp-1(ok554)* allele placed in *trans* to a deficiency chromosome (nDf17) was rescued by the fosmid expressing the PHD finger region (PHD1-PHD2::FLAG) (Avgousti *et al.* 2013), which indicates that the transgenic construct PHD1-PHD2::FLAG is functional. Combined, these results indicate that the short isoform or the increased dosage of the PHD1-PHD2 portion of the long isoform are not sufficient to rescue the HSN migration defects present in the *zfp-1(ok554)* mutant and that the presence of the long isoform containing both the PHD fingers and the C terminus of the protein is required for proper HSN migration.

ZFP-1 works both parallel to and through DAF-16 to control HSN migration

ZFP-1 has been shown to negatively regulate *pdk-1* expression at multiple developmental stages (Mansisidor *et al.* 2011), including the embryo (Figure 2A). To determine whether the HSN undermigration phenotype present in *zfp-1* loss-of-function mutants was due to a de-repression of *pdk-1* and increased IIS leading to decreased nuclear DAF-16 activity (Figure 2B), we performed an epistasis analysis between *zfp-1* and IIS pathway components. First, we created a double-mutant strain between *zfp-1(ok554)* and the null allele *daf-16(mu86)* (Lin *et al.* 1997) to establish whether DAF-16 is the sole output of ZFP-1 involved in HSN migration. We observed a significant enhancement of the *daf-16(mu86)* HSN undermigration phenotype, indicating that the undermigration phenotype caused by a loss of *zfp-1* activity may not be due exclusively to decreased DAF-16 activity (Figure 2C).

Next, we asked whether or not the HSN undermigration defects in *zfp-1(ok554)* could be contributed, in part, to reduced DAF-16 activity due to increased *pdk-1* expression. We performed epistasis analysis between the *pdk-1(sa709)* loss-of-function mutant (Paradis *et al.* 1999; Mansisidor *et al.* 2011) and the *zfp-1(ok554)* mutant to determine whether decreasing *pdk-1* expression in the *zfp-1* mutant background could suppress the HSN undermigration defects. We observed full suppression of the HSN undermigration defects in the double mutant (Figure 2D), suggesting that repression of *pdk-1* by ZFP-1 plays a significant role in regulating HSN migration.

To further demonstrate that enhanced IIS in the *zfp-1 (ok554)* mutant is responsible for inhibiting HSN migration, we also performed epistasis analysis between *zfp-1(ok554)* and *age-1(hx546)*/PI3K reduction-of-function mutants (Friedman and Johnson 1988; Tissenbaum and Ruvkun 1998). Similar to our analysis of *pdk-1* and *zfp-1* mutants, we also observed a full suppression of HSN undermigration defects in *age-1*; *zfp-1* double mutants (Figure 2E). To determine whether the suppression of the *zfp-1* mutant phenotype in IIS pathway mutants was due to a release of DAF-16 inhibition, we created a triple mutant: *daf-16(mu86)*; *age-1 (hx546)*; *zfp-1(ok554)* to remove *daf-16* activity from the *age-1*; *zfp-1* double mutant. We determined that a loss of *daf-16* activity in the *age-1*; *zfp-1* double-mutant background now prevented the suppression of the *zfp-1(ok554)* mutant phenotype by *age-1(hx546)* (Figure 2E). Together, these results suggest that the negative regulation of the IIS pathway by ZFP-1 contributes to the control of HSN migration in a DAF-16-dependent manner.

Since the phenotype of the *zfp-1(ok554)* allele is fully suppressed by mutations in *pdk-1* and *age-1* (Figure 2, D and E), we can attribute the HSN undermigration seen in the *zfp-1(ok554)* mutant solely to reduced DAF-16 activity. However, the genetic enhancement observed in the *daf-16*; *zfp-1* double mutant reveals an additional function for ZFP-1 in parallel with DAF-16, which becomes more essential for proper HSN migration in the absence of DAF-16. Given that both DAF-16 and ZFP-1 regulate transcription, it is likely that they are involved in the regulation of common downstream target genes, which ultimately affect HSN migration.

zfp-1(ok554) limits DAF-16 nuclear localization in the embryonic hypodermis

To investigate the effect of the negative regulation of *pdk-1* by ZFP-1 on DAF-16 subcellular localization during HSN migration, we examined expression of the DAF-16b::TagRFP protein from a transgene driven by the *dpy-7* hypodermal promoter (Kennedy *et al.* 2013) in the *zfp-1(ok554)* mutant background. Previously, we showed that DAF-16 localizes to the hypodermal nuclei in the embryo to promote HSN migration (Kennedy *et al.* 2013). Therefore, we reasoned that if negative regulation of *pdk-1* by ZFP-1 during HSN migration contributes to inhibition of IIS to promote nuclear DAF-16 activity, then, in the *zfp-1* mutant, nuclear localization of DAF-16 should be affected. We find that, in the wild-type background, hypodermally expressed DAF-16 is predominantly nuclear during the comma, 1.5-, and 2-fold stages, when HSN migration is occurring (Sulston *et al.* 1983; Pan *et al.* 2006), and then it becomes cytoplasmically and/or perinuclearly

over a deficiency allele, *nDf17*, also resulted in HSN undermigration defects. Quantification of the percentage of animals with an undermigrated HSN in control animals [*rde-4(ne299)*/qC1] (n = 22) *vs.* *rde-4(ne299)*/nDf17 animals (n = 26). (D) RDE-4 works in parallel to DAF-16 to regulate HSN migration. Quantification of the percentage of animals with an undermigrated HSN from a minimum of two pooled independent experiments per strain in control *tph-1*::*gfp* (n = 127) *vs.* *daf-16(mu86)* (n = 150), *rde-4(ne299)* (n = 211) and *daf-16(mu86)*; *rde-4(ne299)* (n = 270) mutant animals. (E) A *pdk-1* loss-of-function mutant does not suppress *rde-4* null HSN undermigration defects. Quantification of the percentage of animals with an undermigrated HSN in control *tph-1*::*gfp* (n = 64) *vs.* *rde-4(ne299)* (n = 50), *rde-4(ne299)*; *pdk-1(sa709)* (n = 60). (F) An *age-1* loss-of-function mutant does not suppress *rde-4* null HSN undermigration defects. Quantification of the percentage of animals with an undermigrated HSN in control *tph-1*::*gfp* (n = 50) *vs.* *rde-4(ne299)* (n = 50) and *age-1(hx546)*; *rde-4(ne299)* mutant animals. HSNs were visualized with a *tph-1*::*gfp* reporter. See Figure 1 for detailed description of worm schematic legend. ***$P < 0.001$, N.S., not significant (z-test). Error bars represent SEP.

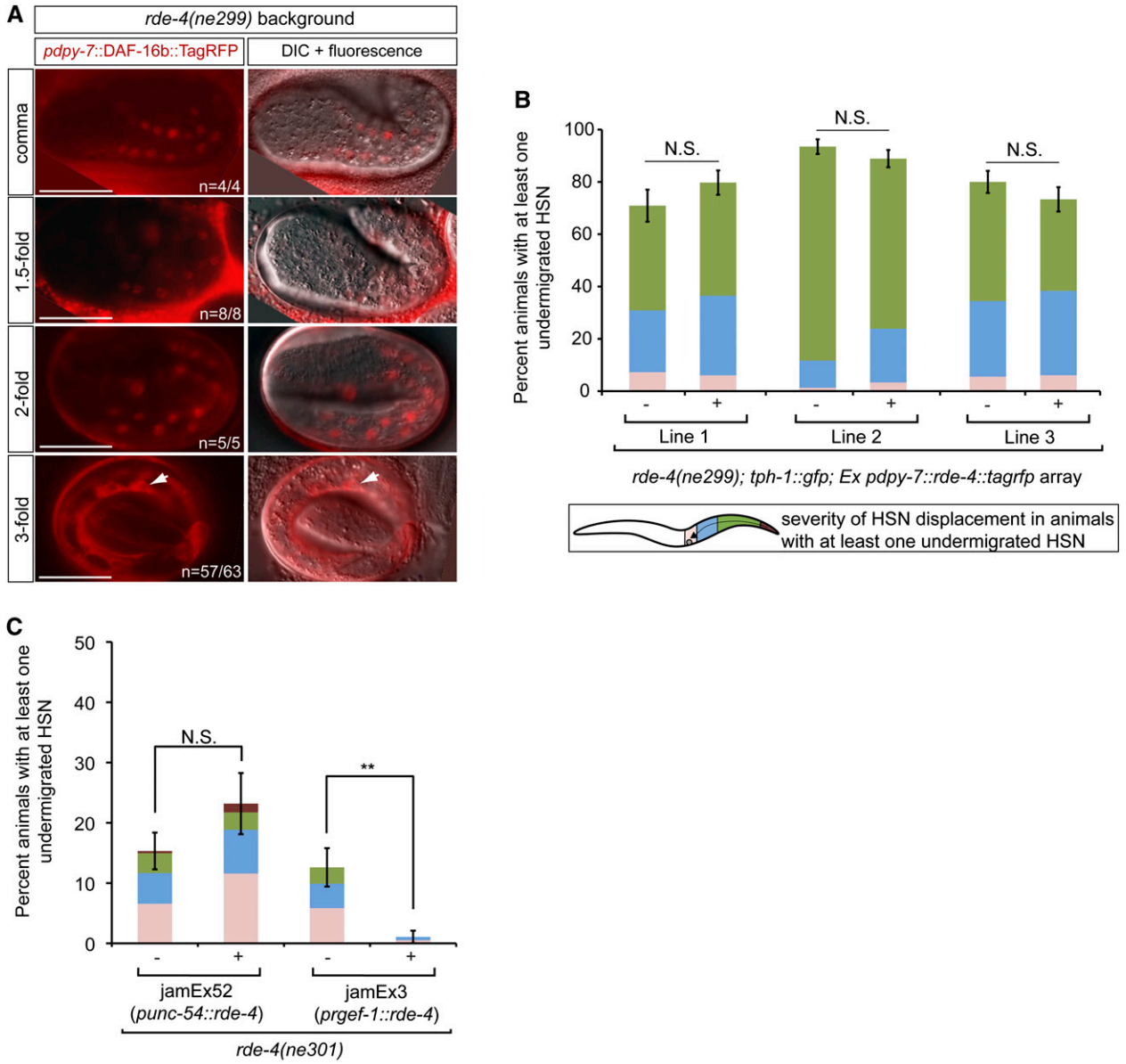

Figure 5 RDE-4 functions in neurons to promote HSN migration. (A) In *rde-4(ne299)* null animals, the distribution of DAF-16b::TagRFP expressed from a hypodermal promoter is unchanged when compared to wild-type embryos (see Figure 3A, left panels). The distribution remains localized to the hypodermal nuclei during the comma, 1.5-, and 2-fold embryonic stages when HSN migration is occurring and is mostly cytoplasmic or perinuclear during the 3-fold stage. Note that in a few 3-fold embryos (6/63), we observed persistent nuclear localization of DAF-16b::TagRFP. The arrows in the 3-fold panels highlight the cytoplasmic/perinuclear localization of DAF-16b::TagRFP in the remaining 57 of the 63 embryos. Bars, 20 μm. (B) Expression of RDE-4 driven by the *dpy-7* promoter does not rescue the HSN undermigration defect in *rde-4(ne299)* mutants. The *rde-4(ne299)* mutants that had the rescuing array (+) or their siblings that had lost the array (−) were scored. Number of animals scored per line are the following: line 1, (−) n = 55 and (+) n = 74; line 2, (−) n = 77 and (+) = 90; line 3, (−) n = 90 and (+) = 90. (C) Expression of RDE-4 driven by a pan-neuronal promoter (*rgef-1*) but not a body-wall muscle promoter (*unc-54*) rescues the HSN migration defect of *rde-4(ne301)* mutants. The *rde-4(ne301)* mutants that carried either the *punc-54*::*rde-4* or *prgef-1*::*rde-4* array (+) and their corresponding siblings that had lost the array (−) were scored. Number of animals scored for the *punc-54*::*rde-4*-containing strain are the following: (+) n = 69 and (−) n = 137. Number of animals scored for the *prgef-1*::*rde-4*-containing strain are the following: (+) n = 93 and (−) n = 111. HSNs were visualized by anti-serotonin staining. See Figure 1 for detailed description of worm schematic legend. $^{**}P < 0.01$, N.S., not significant (*z*-test). Error bars represent SEP.

localized by the 3-fold stage (Figure 3A, left panels). In fact, we have recently reported the finding that dynamic nuclear localization of DAF-16 takes place in the embryonic hypodermal tissue during normal development (Kennedy *et al.* 2013). In the *zfp-1(ok554)* mutant background, although hypodermally expressed DAF-16 is initially nuclearly localized during the comma and 1.5-fold stage (Figure 3A, right panels), it becomes restricted from the nucleus prematurely by the 2-fold stage (Figure 3A, right panels). This result suggests that the change in DAF-16 nuclear localization at the 2-fold stage is responsible for the HSN migration defects observed in the *zfp-1(ok554)* mutant.

As predicted by our epistasis analysis between *pdk-1* and *zfp-1* for the HSN undermigration phenotype (Figure 2D), the *pdk-1(sa709)* loss-of-function mutant also suppresses the change in DAF-16 nuclear localization in *zfp-1(ok554)* mutant embryos (Figure 3, A and B, right panels). First, we confirmed that, consistent with a release of DAF-16 nuclear inhibition under conditions of reduced insulin/IGF-1 signaling, the DAF-16 nuclear localization is more prominent in the *pdk-1 (sa709)* loss-of-function mutant compared to wild-type embryos (Figure 3, A and B, left panels). Specifically, we find that DAF-16 remains nuclear localized throughout the threefold stage in 30 of 72 *pdk-1(sa709)* embryos (42%) (Figure 3B, left panels) compared to 0 of >80 wild-type embryos (Figure 3A, left panels). Next, we determined that in *zfp-1(ok554)*; *pdk-1(sa709)* double-mutant two- and threefold embryos that the subcellular localization of DAF-16 is shifted toward greater nuclear localization when compared to the *zfp-1(ok554)* single mutant (Figure 3, A and B, right panels). The loss-of-function *pdk-1* mutant does not fully suppress the absence of DAF-16 nuclear localization observed in *zfp-1(ok554)* twofold embryos (Figure 3A, right panels) when compared to localization in wild-type embryos at this stage (Figure 3A, left panels) since both nuclear and cytoplasmic localization is often observed in the same embryo in *zfp-1(ok554)*; *pdk-1(sa709)*. However, we reason that even partial restoration of nuclear localization of DAF-16 at the twofold stage in the *zfp-1(ok554)* mutant is sufficient to activate downstream DAF-16 target genes required for HSN migration. We also note that a significant number (33%) of *zfp-1(ok554)*; *pdk-1(sa709)* embryos exhibit the persistence of nuclear DAF-16 at the threefold stage (Figure 3B, right), which is consistent with *pdk-1 (sa709)* being epistatic to *zfp-1(ok554)*.

In total, these results suggest that ZFP-1 functions nonautonomously in the hypodermis to negatively regulate IIS and modulate DAF-16 nuclear localization during HSN migration. Consistently, we also find that the cDNA of the long isoform of *zfp-1* fused to GFP driven by the *unc-86* promoter, which is expressed in a subset of neurons including the HSN (Baumeister *et al.* 1996), does not rescue the HSN undermigration defects seen in *zfp-1(ok554)* mutants (Figure S2, A and B). Interestingly, a conserved microRNA has also been recently reported to function nonautonomously in the hypodermis to regulate genes required for proteoglycan biosynthesis to ensure proper HSN migration (Pedersen *et al.* 2013). Overall, the action of ZFP-1 in controlling DAF-16 dynamics in the hypodermis that we describe here complements well our earlier findings of the nonautonomous roles of both DAF-16 and DAF-18 (PTEN) in regulating HSN migration (Figure 2B) (Kennedy *et al.* 2013).

RNAi factors RDE-4, DRH-3, and CSR-1 regulate HSN migration

A genome-wide expression study has revealed that ZFP-1 and RDE-4, a dsRNA-binding protein required for the initiation of exogenous RNAi (Parrish and Fire 2001; Tabara *et al.* 2002), regulate close to 250 overlapping genes (Grishok *et al.* 2008). Consistent with this finding, both RDE-4 and ZFP-1 have been shown to affect longevity and the stress response by negatively regulating the conserved IIS kinase *pdk-1* (Mansisidor *et al.* 2011). Therefore, we examined a null allele of *rde-4* (Tabara *et al.* 2002), as well as mutants in 11 other RNAi components that represent multiple small RNA pathways [*i.e.*, CSR-1, WAGO, ERI (enhanced RNA1), microRNA, and nuclear and exogenous RNAi (reviewed in Grishok 2013)] for defects in HSN migration (Table 1). We crossed RNAi mutants to a *tph-1*::*gfp* reporter strain and identified three mutants that display HSN migration defects: the *rde-4(ne299)* null mutant (Tabara *et al.* 2002), the *drh-3(ne4253)* loss-of-function mutant (Gu *et al.* 2009), and a *csr-1(tm892)* partially rescued strain (Claycomb *et al.* 2009) (Table 1 and Figure 4, A and B). Strikingly, the highest percentage of undermigration defects was observed in *rde-4* null mutants, with almost all affected animals exhibiting migration defects in both HSNs, as shown by the relatively small proportion of HSNs in the wild-type position (Figure 4B, pink in stack). Also, in addition to the undermigration defect observed in 16% of the *drh-3(ne4253)* mutant animals (Figure 4B), we also noted a smaller percentage of animals with an overmigration defect (~9%). *drh-3* encodes a **d**icer-**r**elated **h**elicase, which participates in multiple endogenous RNAi pathways in *C. elegans* (Gu *et al.* 2009), and *csr-1* encodes an Argonaute, which binds 22G-RNAs antisense to protein-coding genes (Claycomb *et al.* 2009; Gu *et al.* 2009). Consistent with only a reduction of function in the *drh-3* and *csr-1* mutants, fewer animals exhibited HSN undermigration defects compared to the *rde-4* null mutant (Figure 4B). We used a *drh-3* loss-of-function allele since null mutants are infertile (Gu *et al.* 2009). Since *csr-1(tm892)* mutants are also sterile, we used a partially rescued transgenic strain, where CSR-1 is expressed in the germline to produce 38% viable progeny (Claycomb *et al.* 2009) that we could analyze for migration defects.

To further confirm that the HSN undermigration defect that we observed in *rde-4* null mutants is due to mutations in *rde-4* and not to the background of the strain, we placed the *rde-4(ne299)* allele over a deficiency allele, *nDf17*, which is balanced by chromosome qC1 [*dpy-19(e1259) glp-1(q339)*] (Edgley *et al.* 2006). We crossed *rde-4 (ne299)* males to nDf17/qC1 animals and scored F_1 animals for HSN migration defects. We determined the genotypes of the F_1 animals by the presence or absence of the qC1 phenotypes, which are dumpy and sterile, segregating in the F_2 generation. Only F_1 animals carrying the deficiency allele *nDf17* displayed penetrant HSN undermigration defects (Figure 4C). Moreover, we also stained *rde-4(ne299)* worms with an anti-serotonin antibody (Garriga *et al.* 1993) to further exclude the possibility that the HSN undermigration defects observed in *rde-4* null animals were the result of transgene background effects. We observed HSN undermigration defects in stained worms without the *tph-1*::*gfp* transgene (Figure S3, A and B). Similar to *zfp-1* mutants,

Table 1 RNAi mutants surveyed for HSN migration defect

RNAi pathway gene	Class	Nature of mutation	HSN migration defect?
alg-1 (gk214)	Argonaute	Loss of function[a]	No
C04f12.1 (tm892)	Argonaute	Loss of function[b]	No
csr-1 (tm892)	Nuclear Argonaute	Partially rescued mutant[c]	Yes
drh-3 (ne4253)	Helicase	Loss of function[d]	Yes
ergo-1 (tm1860)	Argonaute	Loss of function[b]	No
nrde-3 (gg066)	Nuclear Argonaute	Null[e]	No
rde-1 (ne300)	Argonaute	Putative null[f]	No
rde-3 (ne298)	Nucleotidyl-transferase	Loss of function[f]	No
rde-4 (ne299)	dsRNA binding	Null[f]	Yes
rrf-1 (pk1417)	RdRP	Null[g]	No
rrf-2 (ok210)	RdRP	Null[h]	No
rrf-3 (pk1426)	RdRP	Null[g]	No

HSNs were visualized by crossing a *tph-1*::*gfp* reporter into individual mutant strains.
[a] Grishok *et al.* (2005).
[b] Yigit *et al.* (2006).
[c] Claycomb *et al.* (2009).
[d] Gu *et al.* (2009).
[e] Guang *et al.* (2008).
[f] Tabara *et al.* (1999).
[g] Sijen *et al.* (2001).
[h] Deletion allele provided by the *C. elegans* Gene Knockout Project. The deletion covers part of the expected promoter region and the first two exons.

rde-4 mutants are not affected in the production of serotonin since undermigrated HSNs contain the neurotransmitter.

RDE-4 works in parallel to DAF-16 and in the neuronal tissue to regulate HSN migration

Since RDE-4 was shown to inhibit *pdk-1* transcription (Mansisidor *et al.* 2011), we analyzed epistatic relationships between the *rde-4* mutant and IIS pathway components to determine if RDE-4, like ZFP-1, also regulates HSN migration in part by inhibiting IIS to promote DAF-16 nuclear localization. First, we combined the *rde-4(ne299)* null allele with the *daf-16(mu86)* null allele and observed a significant enhancement of the *daf-16* null phenotype (Figure 4D). This result suggests that *rde-4* and *daf-16* are working in parallel genetic pathways to affect HSN migration.

Since we found that the *zfp-1* mutant phenotype can be suppressed by a reduction in *pdk-1* and *age-1* expression, we also performed epistasis analysis using *rde-4(ne299)* and either the *pdk-1(sa709)* mutant or the *age-1(hx546)* mutant to determine if the HSN undermigration phenotype seen in *rde-4(ne299)* could also be suppressed by reduced IIS. In contrast to the epistasis experiments with *zfp-1*, we observed no suppression of the HSN undermigration defects in either double-mutant combination (Figure 4, E and F).

In addition, we have analyzed the cellular distribution of hypodermally expressed DAF-16b::TagRFP in *rde-4(ne299)* null mutant embryos (Figure 5A) and found it to be similar to that observed in the wild-type background (Figure 3A, left panels): DAF-16 is predominantly nuclear during the comma, 1.5-, and 2-fold stages when HSN migration is occurring before becoming more restricted to the cytoplasm (Figure 5A). The absence of any alterations in DAF-16 nuclear localization during HSN migration in the *rde-4* mutant background compared to wild type is consistent with the lack of suppression that we observe for the HSN undermigration defect in the *rde-4(ne299)*; *pdk-1(sa709)* double mutant (Figure 4E). Combined, these results indicate that RDE-4 does not contribute to the regulation of HSN migration by promoting hypodermal DAF-16 nuclear localization during embryogenesis. Consistently, we also find that the cDNA of *rde-4* fused to TagRFP driven by the hypodermal promoter *dpy-7* fails to rescue the HSN undermigration defects seen in the *rde-4* null mutant (Figure 5B).

To determine the site of action of RDE-4 in HSN migration, we utilized two different functional tissue-specific *rde-4* transgenes (A. Jose, personal communication). The *rde-4* cDNA was driven by either a body-wall muscle promoter, *unc-54*, or a pan-neuronal promoter, *rgef-1*, in the *rde-4 (ne301)* null mutant background (strains were generously provided by the A. Jose lab). Expression of *rde-4* cDNA in the neuronal tissue but not in the body-wall muscle rescued the HSN migration defects of *rde-4* mutants (Figure 5C). This result suggests that RDE-4 functions cell-autonomously to control HSN migration and is in agreement with our findings that RDE-4 does not function in the same genetic pathway or tissue as DAF-16.

We observed that the HSN undermigration defect is less severe in the genetic background of the two *rde-4* mutant strains expressing the extrachromosomal muscle- and neuronal-specific transgenes (Figure 5C) compared to the strains used throughout the rest of this study. We have used strains containing the *rde-4(ne299)* allele while the strains from the Jose lab contain the *rde-4(ne301)* allele. Although these two alleles contain an identical lesion and were isolated from a clonal population during a screen for RNAi-defective mutants (Tabara *et al.* 1999), they have been maintained and outcrossed independently. As a result, they may have slightly different genetic backgrounds accounting

for the variability in HSN undermigration defects observed between the two *rde-4* alleles.

Discussion

Our genetic analysis has identified the conserved chromatin-binding factor ZFP-1/AF10, the dsRNA-binding protein RDE-4, the dicer-related helicase DRH-3, and the Argonaute CSR-1 as regulators of neuronal migration during *C. elegans* embryogenesis. We demonstrate that ZFP-1 facilitates proper HSN migration in part through its negative regulation of the conserved IIS kinase gene *pdk-1* (Mansisidor *et al.* 2011) and the resulting activation of DAF-16/FOXO, which we have previously shown to act in the hypodermis to promote HSN migration (Kennedy *et al.* 2013). We also show that both ZFP-1 and RDE-4 work in parallel to DAF-16 to stimulate HSN migration during embryogenesis.

Recently, the mammalian homolog of ZFP-1, AF10, was shown to exist in a complex with the H3K79 histone methyltransferase DOT1L, which was called DotCom (Mohan *et al.* 2010). Interestingly, β-catenin, an important downstream mediator of Wnt signaling, was shown to co-immunoprecipitate with DOT1L complex components in HEK293T cells (Mohan *et al.* 2010). Moreover, reduced expression of Wingless/Wnt targets was observed after knockdown of the fly AF10 ortholog *Alhambra* (or *Dalf*), as well as after the knockdown of other DotCom orthologs, in *Drosophila* larvae (Mohan *et al.* 2010). Additionally, AF10 was independently found in a complex with the downstream effectors of Wnt signaling TCF4 and β-catenin in colorectal cancer cells and implicated in the regulation of Wnt target genes in these cells as well as in zebrafish (Mahmoudi *et al.* 2010).

In *C. elegans*, it is well known that Wnt signaling controls HSN migration in a β-catenin-independent manner (Harris *et al.* 1996; Forrester *et al.* 2004) by acting as a repellent to guide the HSN out of the embryonic tail and into the mid-body of the animal (Pan *et al.* 2006). However, the connection between AF10 and canonical Wnt signaling (β-catenin-dependent) in vertebrates highlights the intriguing possibility that the interaction between ZFP-1/AF10 and Wnt pathway components may be conserved in *C. elegans*. Based on our observations that the negative regulation of *pdk-1* by ZFP-1 affects DAF-16 hypodermal nuclear localization during HSN migration and that an HSN-specific promoter driving the expression of a ZFP-1::GFP transgene fails to rescue the HSN undermigration defects in *zfp-1* mutant animals, it is likely that ZFP-1 functions nonautonomously to promote HSN migration. One possibility is that ZFP-1, independently or in combination with DAF-16, regulates the transcription of the Wnt's, which affect HSN migration nonautonomously (Pan *et al.* 2006). Another possibility is that ZFP-1 regulates the transcription of negative regulators of Wnt signaling, such as CAM-1, that can function as sinks to limit extracellular Wnt's and impede HSN migration (Kim and Forrester 2003; Forrester *et al.* 2004; Green *et al.* 2007). Future studies will elucidate these potential roles of ZFP-1 in the regulation of Wnt signaling during HSN migration.

There are multiple endo-siRNA pathways in *C. elegans*, including the CSR-1 RNAi pathway (Claycomb *et al.* 2009; Gu *et al.* 2009), the WAGO RNAi pathway (Gu *et al.* 2009), and the ERI RNAi pathway (Lee *et al.* 2006; Gent *et al.* 2009; Han *et al.* 2009; Vasale *et al.* 2010). The biological roles of the endo-RNAi pathways in *C. elegans* remain largely uncharacterized. A major known role of the WAGO endo-RNAi pathway is in genome surveillance: the silencing of transposable elements, aberrant transcripts (Gu *et al.* 2009), and gene duplications (Vasale *et al.* 2010; Fischer *et al.* 2011). The ERI pathway has been implicated in regulating genes required for spermatogenesis and fertility (Gent *et al.* 2009; Han *et al.* 2009; Conine *et al.* 2010), whereas the CSR-1 RNAi pathway has been recently shown to positively regulate histone mRNA expression (Avgousti *et al.* 2012).

Mutations in *rde-4* have been associated with decreased life span (Welker *et al.* 2007; Mansisidor *et al.* 2011) and increased sensitivity to oxidative stress (Mansisidor *et al.* 2011) and temperature (Blanchard *et al.* 2011). An increase in stress sensitivity and reduced life span of *rde-4* mutants has been attributed to the upregulation of *pdk-1* (Mansisidor *et al.* 2011). Here, we describe a novel role for RDE-4 in embryonic neuronal migration, which is consistent with previous observations that the generation of some somatic 22G-RNAs is dependent on RDE-4 (Lee *et al.* 2006; Gu *et al.* 2009). Interestingly, RDE-4 has also been recently shown to participate in the production of endogenous 22G-RNAs required to mediate odor adaptation in adult animals (Juang *et al.* 2013).

The majority of 22G-RNAs that are in the complex with the Argonaute CSR-1 are antisense to protein-coding genes (Claycomb *et al.* 2009), suggesting that multiple genes and genetic pathways may be regulated by these endo-siRNAs. Similar to the regulation of embryonic HSN migration described here, both CSR-1 and DRH-3 have been implicated in another embryonic process: the specification of the excretory duct cell, a component of the worm's renal system (Rocheleau *et al.* 2008). A genome-wide RNAi screen identified these RNAi pathway genes to act redundantly with the KSR-1 (**k**inase **s**uppressor of **R**as) scaffolding protein in Ras-mediated excretory duct cell specification (Rocheleau *et al.* 2008). Since DRH-3 is a component of the RdRP complex (Gu *et al.* 2009; Thivierge *et al.* 2012) required for the biogenesis of all 22G-RNAs, including those present in the complex with CSR-1 (Gu *et al.* 2009), it is most likely that DRH-3-dependent CSR-1-bound endo-siRNAs regulate a number of genes affecting developmental events, such as HSN migration and excretory duct specification.

Furthermore, RDE-4 and Dicer have been implicated in the production of 26G-RNAs, which subsequently promote RdRP-dependent, Dicer-independent biogenesis of some WAGO-bound 22G-RNAs (Vasale *et al.* 2010). Therefore, it is possible that RDE-4 works upstream of some CSR-1 22G-RNAs that regulate genes affecting HSN migration.

Surprisingly, none of the RdRPs implicated in 26G-RNA and 22G-RNA production (Ruby *et al.* 2006; Aoki *et al.* 2007; Pak and Fire 2007; Vasale *et al.* 2010) displayed an HSN migration phenotype when examined as null mutants (Table 1). One possible explanation for this is redundancy among the RdRPs required for HSN migration.

In summary, our work has highlighted a novel biological role for the conserved chromatin-binding factor ZFP-1/AF10 and the endo-siRNA pathway in neuronal migration in *C. elegans*.

Acknowledgments

We thank I. Greenwald, O. Hobert, and members of the Grishok lab for helpful discussions; G. Cecere and A. Mansisidor for generating the fosmid-based transgenic strains; M. Hengartner and S. Gysi for providing the *zfp-1 (op481)* allele and for sharing data before publication; A. Jose for providing *rde-4* transgenic strains; X. Zhou for help in generating plasmid-based transgenic lines; and I. Greenwald for a generous offer of technical assistance by her staff. The *zfp-1(ok554)* and *rrf-2(ok210)* strains were provided by the *C. elegans* Gene Knockout Project at the Oklahoma Medical Research Foundation, which is part of the International *C. elegans* Gene Knockout Consortium. Some strains were provided by the Caenhorhabditis Genetics Center, which is funded by the National Institutes of Health (NIH) Office of Research Infrastructure Programs (P40 0D010440). The *ergo-1(tm1860)*, *C04F12.1(tm1637)*, and *csr-1(tm892)* alleles were generated by the National Bioresource Project (Japan). This work was supported by Hormones: Biochemistry and Molecular Biology Training Grant T32 DK0007328 and Genetics and Development Training Grant T32 GM007088 (to L.M.K.) and NIH Director's New Innovator Award (1DP2OD006412-01) and the Irma T. Hirschl Career Scientist Award (to A.G.).

Literature Cited

Aoki, K., H. Moriguchi, T. Yoshioka, K. Okawa, and H. Tabara, 2007 In vitro analyses of the production and activity of secondary small interfering RNAs in C. elegans. EMBO J. 26: 5007–5019.

Avgousti, D. C., S. Palani, Y. Sherman, and A. Grishok, 2012 CSR-1 RNAi pathway positively regulates histone expression in C. elegans. EMBO J. 31: 3821–3832.

Avgousti, , D. C., G Cecere, and A Grishok, 2013 The conserved PHD1-PHD2 domain of ZFP-1/AF10 is a discrete functional module essential for viability in Caenorhabditis elegans. Mol. Cell. Biol. 33: 999–1015.

Baumeister, R., Y. Liu, and G. Ruvkun, 1996 Lineage-specific regulators couple cell lineage asymmetry to the transcription of the Caenorhabditis elegans POU gene unc-86 during neurogenesis. Genes Dev. 10: 1395–1410.

Blanchard, D., P. Parameswaran, J. Lopez-Molina, J. Gent, J. F. Saynuk *et al.*, 2011 On the nature of in vivo requirements for rde-4 in RNAi and developmental pathways in C. elegans. RNA Biol. 8: 458–467.

Brenner, S., 1974 The genetics of *Caenorhabditis elegans*. Genetics 77: 71–94.

Cecere, G., S. Hoersch, M. B. Jensen, S. Dixit, and A. Grishok, 2013 The ZFP-1(AF10)/DOT-1 complex opposes H2B ubiquitination to reduce Pol II transcription. Mol. Cell 50: 894–907.

Chaplin, T., P. Ayton, O. A. Bernard, V. Saha, V. Della Valle *et al.*, 1995 A novel class of zinc finger/leucine zipper genes identified from the molecular cloning of the t(10;11) translocation in acute leukemia. Blood 85: 1435–1441.

Clark, S. G., and C. Chiu, 2003 C. elegans ZAG-1, a Zn-finger-homeodomain protein, regulates axonal development and neuronal differentiation. Development 130: 3781–3794.

Claycomb, J. M., P. J. Batista, K. M. Pang, W. Gu, J. J. Vasale *et al.*, 2009 The Argonaute CSR-1 and its 22G-RNA cofactors are required for holocentric chromosome segregation. Cell 139: 123–134.

Conine, C. C., P. J. Batista, W. Gu, J. M. Claycomb, D. A. Chaves *et al.*, 2010 Argonautes ALG-3 and ALG-4 are required for spermatogenesis-specific 26G-RNAs and thermotolerant sperm in Caenorhabditis elegans. Proc. Natl. Acad. Sci. USA 107: 3588–3593.

Cui, M., E. Kim, and M. Han, 2006 Diverse chromatin remodeling genes antagonize the Rb-involved SynMuv pathways in C. elegans. PLoS Genet. 2: e74.

Desai, C., G. Garriga, S. L. McIntire, and H. R. Horvitz, 1988 A genetic pathway for the development of the Caenorhabditis elegans HSN motor neurons. Nature 336: 638–646.

DiMartino, J. F., P. M. Ayton, E. H. Chen, C. C. Naftzger, B. D. Young *et al.*, 2002 The AF10 leucine zipper is required for leukemic transformation of myeloid progenitors by MLL-AF10. Blood 99: 3780–3785.

Dudley, N. R., J. C. Labbe, and B. Goldstein, 2002 Using RNA interference to identify genes required for RNA interference. Proc. Natl. Acad. Sci. USA 99: 4191–4196.

Edgley, M. L., D. L. Baillie, D. L. Riddle, and A. M. Rose, 2006 Genetic balancers (April 6, 2006), WormBook, ed. The C. elegans Research Community, WormBook, doi/10.1895/wormbook.1.89.1, http://www.wormbook.org.

Fischer, S. E., T. A. Montgomery, C. Zhang, N. Fahlgren, P. C. Breen *et al.*, 2011 The ERI-6/7 helicase acts at the first stage of an siRNA amplification pathway that targets recent gene duplications. PLoS Genet. 7: e1002369.

Forrester, W. C., C. Kim, and G. Garriga, 2004 The *Caenorhabditis elegans* Ror RTK CAM-1 inhibits EGL-20/Wnt signaling in cell migration. Genetics 168: 1951–1962.

Friedman, , D. B., and T. E Johnson, 1988 A mutation in the *age-1* gene in *Caenorhabditis elegans* lengthens life and reduces hermaphrodite fertility. Genetics 118: 75–86.

Garriga, G., C. Desai, and H. R. Horvitz, 1993 Cell interactions control the direction of outgrowth, branching and fasciculation of the HSN axons of Caenorhabditis elegans. Development 117: 1071–1087.

Gent, J., M. Schvarzstein, A. M. Villeneuve, S. G. Gu, V. Jantsch *et al.*, 2009 A *Caenorhabditis elegans* RNA-directed RNA polymerase in sperm development and endogenous RNA interference. Genetics 183: 1297–1314.

Gilleard, , J. S., J. D Barry, and I. L Johnstone, 1997 cis regulatory requirements for hypodermal cell-specific expression of the Caenorhabditis elegans cuticle collagen gene dpy-7. Mol. Cell. Biol. 17: 2301–2311.

Green, J. L., T. Inoue, and P. W. Sternberg, 2007 The C. elegans ROR receptor tyrosine kinase, CAM-1, non-autonomously inhibits the Wnt pathway. Development 134: 4053–4062.

Grishok, A., 2013 Biology and mechanisms of short RNAs in Caenorhabditis elegans. Adv. Genet. 83: 1–69.

Grishok, A., J. L. Sinskey, and P. A. Sharp, 2005 Transcriptional silencing of a transgene by RNAi in the soma of C. elegans. Genes Dev. 19: 683–696.

Grishok, A., S. Hoersch, and P. A. Sharp, 2008 RNA interference and retinoblastoma-related genes are required for repression of endogenous siRNA targets in Caenorhabditis elegans. Proc. Natl. Acad. Sci. USA 105: 20386–20391.

Gu, W., M. Shirayama, D. Conte, J. Vasale, P. J. Batista *et al.*, 2009 Distinct Argonaute-mediated 22G-RNA pathways direct genome surveillance in the C. elegans germline. Mol. Cell 36: 231–244.

Guang, S., A. F. Bochner, D. M. Pavelec, K. B. Burkhart, S. Harding *et al.*, 2008 An Argonaute transports siRNAs from the cytoplasm to the nucleus. Science 321: 537–541.

Gysi, S., C. Rhiner, S. Flibotte, D. G. Moerman, and M. O. Hengartner, 2013 A network of HSPG core proteins and HS modifying enzymes regulates Netrin-dependent guidance of D-type motor neurons in Caenorhabditis elegans. PLoS ONE 8: e74908.

Han, T., A. P. Manoharan, T. T. Harkins, P. Bouffard, C. Fitzpatrick *et al.*, 2009 26G endo-siRNAs regulate spermatogenic and zygotic gene expression in Caenorhabditis elegans. Proc. Natl. Acad. Sci. USA 106: 18674–18679.

Harris, J., L. Honigberg, N. Robinson, and C. Kenyon, 1996 Neuronal cell migration in C. elegans: regulation of Hox gene expression and cell position. Development 122: 3117–3131.

Juang, B. T., C. Gu, L. Starnes, F. Palladino, A. Goga *et al.*, 2013 Endogenous Nuclear RNAi mediates behavioral adaptation to odor. Cell 154: 1010–1022.

Kennedy, L. M., S. C. Pham, and A. Grishok, 2013 Nonautonomous regulation of neuronal migration by insulin signaling, DAF-16/FOXO, and PAK-1. Cell Rep. 4: 996–1009.

Kim, C., and W. C. Forrester, 2003 Functional analysis of the domains of the C elegans Ror receptor tyrosine kinase CAM-1. Dev. Biol. 264: 376–390.

Kim, J. K., H. W. Gabel, R. S. Kamath, M. Tewari, A. Pasquinelli *et al.*, 2005 Functional genomic analysis of RNA interference in C. elegans. Science 308: 1164–1167.

Lee, R. C., C. M. Hammell, and V. Ambros, 2006 Interacting endogenous and exogenous RNAi pathways in Caenorhabditis elegans. RNA 12: 589–597.

Li, L., and Y. Liu, 2011 Diverse small non-coding RNAs in RNA interference pathways. Methods Mol. Biol. 764: 169–182.

Lin, K., J. B. Dorman, A. Rodan, and C. Kenyon, 1997 daf-16: an HNF-3/forkhead family member that can function to double the life-span of Caenorhabditis elegans. Science 278: 1319–1322.

Mahmoudi, T., S. F. Boj, P. Hatzis, V. S. Li, N. Taouatas *et al.*, 2010 The leukemia-associated Mllt10/Af10-Dot1l are Tcf4/beta-catenin coactivators essential for intestinal homeostasis. PLoS Biol. 8: e1000539.

Mansisidor, A. R., G. Cecere, S. Hoersch, M. B. Jensen, T. Kawli *et al.*, 2011 A conserved PHD finger protein and endogenous RNAi modulate insulin signaling in Caenorhabditis elegans. PLoS Genet. 7: e1002299.

Mello, C. C., J. M. Kramer, D. Stinchcomb, and V. Ambros, 1991 Efficient gene transfer in C. elegans: extrachromosomal maintenance and integration of transforming sequences. EMBO J. 10: 3959–3970.

Mohan, M., H. M. Herz, Y. H. Takahashi, C. Lin, K. C. Lai *et al.*, 2010 Linking H3K79 trimethylation to Wnt signaling through a novel Dot1-containing complex (DotCom). Genes Dev. 24: 574–589.

Pak, J., and A. Fire, 2007 Distinct populations of primary and secondary effectors during RNAi in C. elegans. Science 315: 241–244.

Pan, C. L., J. E. Howell, S. G. Clark, M. Hilliard, S. Cordes *et al.*, 2006 Multiple Wnts and frizzled receptors regulate anteriorly directed cell and growth cone migrations in Caenorhabditis elegans. Dev. Cell 10: 367–377.

Paradis, S., M. Ailion, A. Toker, J. H. Thomas, and G. Ruvkun, 1999 A PDK1 homolog is necessary and sufficient to transduce AGE-1 PI3 kinase signals that regulate diapause in Caenorhabditis elegans. Genes Dev. 13: 1438–1452.

Parrish, S., and A. Fire, 2001 Distinct roles for RDE-1 and RDE-4 during RNA interference in Caenorhabditis elegans. RNA 7: 1397–1402.

Pedersen, M. E., G. Snieckute, K. Kagias, C. Nehammer, H. A. Multhaupt *et al.*, 2013 An epidermal microRNA regulates neuronal migration through control of the cellular glycosylation state. Science 341: 1404–1408.

Rocheleau, C., K. Cullison, K. Huang, Y. Bernstein, A. Spilker *et al.*, 2008 The *Caenorhabditis elegans* ekl (Enhancer of ksr-1 Lethality) genes include putative components of a germline small RNA pathway. Genetics 178: 1431–1443.

Ruby, J. G., C. Jan, C. Player, M. J. Axtell, W. Lee *et al.*, 2006 Large-scale sequencing reveals 21U-RNAs and additional microRNAs and endogenous siRNAs in C. elegans. Cell 127: 1193–1207.

Sijen, T., J. Fleenor, F. Simmer, K. L. Thijssen, S. Parrish *et al.*, 2001 On the role of RNA amplification in dsRNA-triggered gene silencing. Cell 107: 465–476.

Sulston, J. E., E Schierenberg, J. G White,, and J. N. Thomson, 1983 The embryonic cell lineage of the nematode Caenorhabditis elegans. Dev. Biol. 100: 64–119.

Tabara, H., M. Sarkissian, W. G. Kelly, J. Fleenor, A. Grishok *et al.*, 1999 The rde-1 gene, RNA interference, and transposon silencing in C. elegans. Cell 99: 123–132.

Tabara, H., E. Yigit, H. Siomi, and C. C. Mello, 2002 The dsRNA binding protein RDE-4 interacts with RDE-1, DCR-1, and a DExH-box helicase to direct RNAi in C. elegans. Cell 109: 861–871.

Thivierge, C., N. Makil, M. Flamand, J. J. Vasale, C. C. Mello *et al.*, 2012 Tudor domain ERI-5 tethers an RNA-dependent RNA polymerase to DCR-1 to potentiate endo-RNAi. Nat. Struct. Mol. Biol. 19: 90–97.

Tissenbaum, H. A., and G. Ruvkun, 1998 An insulin-like signaling pathway affects both longevity and reproduction in *Caenorhabditis elegans*. Genetics 148: 703–717.

Vasale, J. J., W. Gu, C. Thivierge, P. J. Batista, J. M. Claycomb *et al.*, 2010 Sequential rounds of RNA-dependent RNA transcription drive endogenous small-RNA biogenesis in the ERGO-1/Argonaute pathway. Proc. Natl. Acad. Sci. USA 107: 3582–3587.

Welker, N. C., J. W. Habig, and B. L. Bass, 2007 Genes misregulated in C. elegans deficient in Dicer, RDE-4, or RDE-1 are enriched for innate immunity genes. RNA 13: 1090–1102.

Yigit, E., P. J. Batista, Y. Bei, K. M. Pang, C. C. Chen *et al.*, 2006 Analysis of the C. elegans Argonaute family reveals that distinct Argonautes act sequentially during RNAi. Cell 127: 747–757.

Communicating editor: P. Sengupta

GENETICS

Supporting Information
http://www.genetics.org/lookup/suppl/doi:10.1534/genetics.114.162917/-/DC1

Neuronal Migration Is Regulated by Endogenous RNAi and Chromatin-Binding Factor ZFP-1/AF10 in *Caenorhabditis elegans*

Lisa M. Kennedy and Alla Grishok

Copyright © 2014 by the Genetics Society of America
DOI: 10.1534/genetics.114.162917

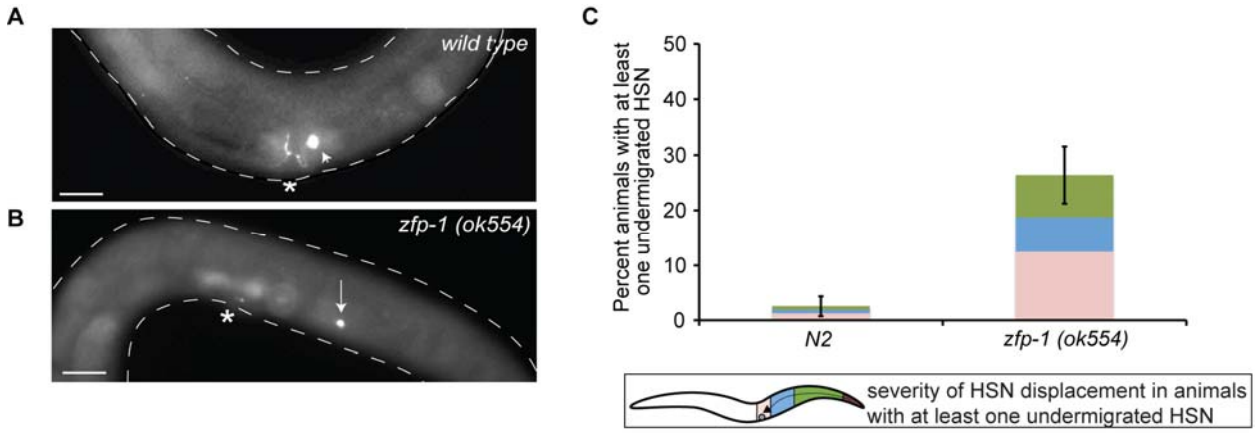

Figure S1 HSN migration defects in *zfp-1(ok554)* determined by anti-serotonin staining. (A) Epifluorescent images of the HSN stained with anti-serotonin in wild type (A) and *zfp-1(ok554)* adult animals (B). Asterisks indicate the vulva and the arrowhead denotes the position of a properly migrated HSN. The arrow in (B) indicates a HSN that has failed to migrate the full distance from its birthplace in the tail of the *zfp-1(ok554)* mutant animal. Note that undermigrated HSNs still differentiate, as they express the neurotransmitter serotonin, a late step in HSN development. Images are oriented with the posterior of the animal to the right. Scale bars: 20 μm. (C) Quantification of the percentage of animals with an undermigrated HSN from two pooled independent experiments in wild type (n=78) versus *zfp-1(ok554)* (n=72) animals. Worm schematic legend: Stacked bars represent the proportion of HSNs at different positions along the A-P body axis within only those animals containing at least one undermigrated HSN. Thus, since there are two HSNs within each animal and not every HSN is affected, one colored region (light pink) represents the wild type HSN that remains unaffected in animals containing a second undermigrated HSN, which is represented by either the reddish/purple, green or blue region. Error bars represent standard error of the proportion (SEP).

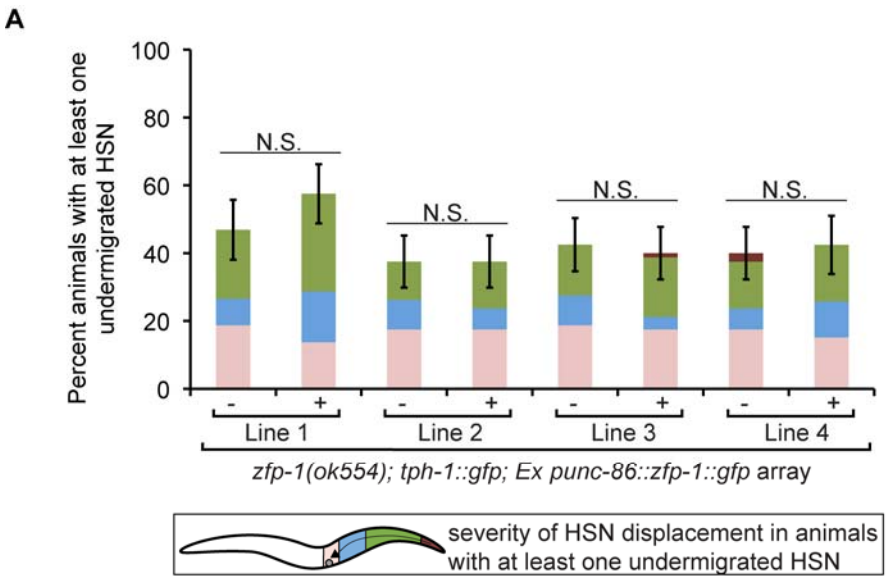

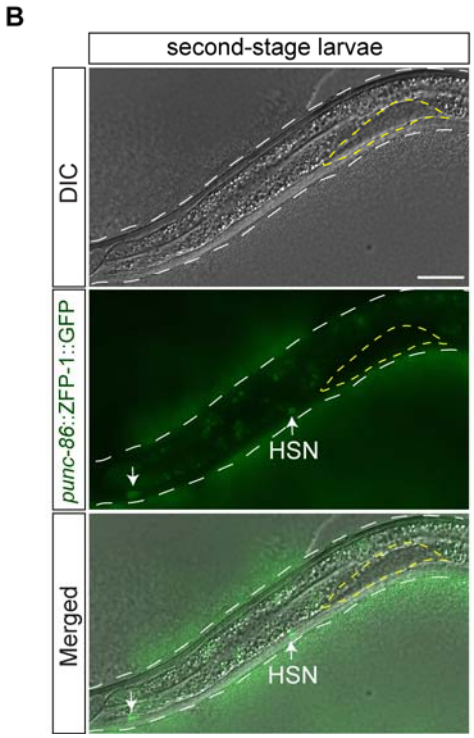

Figure S2 ZFP-1 may function nonautonomously to promote HSN migration. (A) Expression of ZFP-1::GFP in the HSN does not rescue the HSN undermigration defect of *zfp-1(ok554)* mutants. The *zfp-1(ok554)* mutants that had the transgenic array (+) or their siblings that had lost the array (-) were scored. Number of animals scored per line are: Line 1: (-) n=32 and (+) n=40; Line 2: (-) n=40 and (+) n=40; Line 3: (-) n=40 and (+) n=40; Line 4: (-) n=40 and (+) n=33. HSNs were visualized with a *tph-1::gfp* reporter. See Figure S1 for detailed description of worm schematic legend. The *z*-test was used to determine significance. Error bars represent SEP. (B) ZFP-1::GFP driven by the *unc-86* promoter is expressed in a subset of neurons, including the HSN, in *zfp-1(ok554)*. The dotted yellow line represents the developing gonad. The HSN is indicated by an arrow and a second arrow in the tail illustrates a tail neuron, which also expresses ZFP-1::GFP.

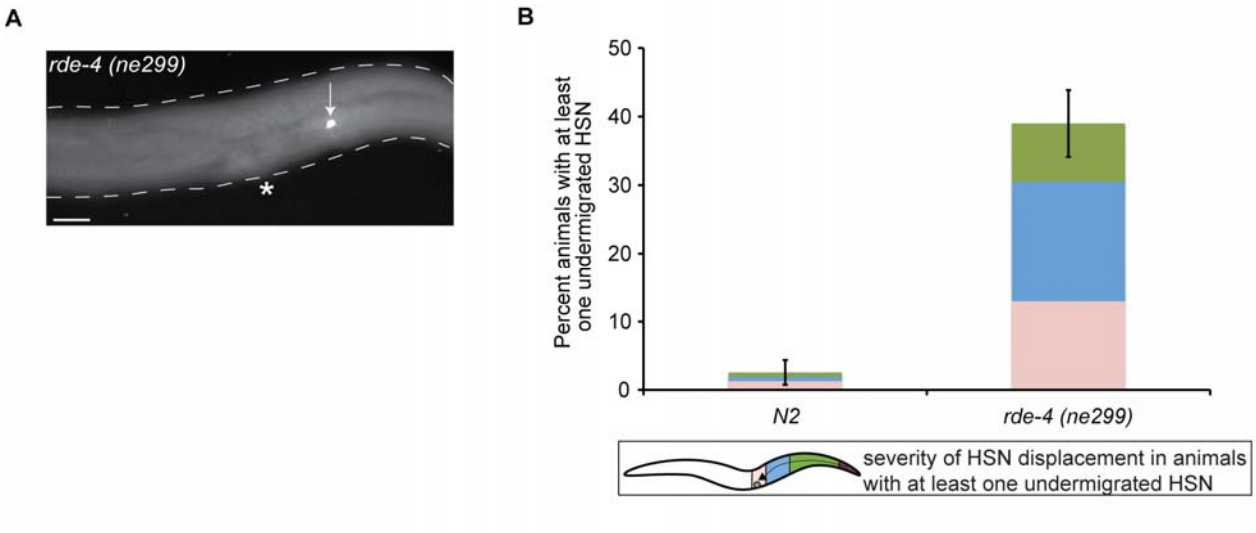

Figure S3 HSN migration defects in *rde-4(ne299)* determined by anti-serotonin staining. (A) Epifluorescent image of the HSN stained with anti-serotonin in *rde-4(ne299)* animals (B). The asterisk indicates the vulva and the arrow indicates a HSN that has failed to migrate the full distance from its birthplace in the tail to flank the vulva. Note that undermigrated HSNs still differentiate, as they express the neurotransmitter serotonin, a late step in HSN development. Image is oriented with the posterior of the animal to the right. Scale bars: 20 μm. (B) Quantification of the percentage of animals with an undermigrated HSN from two pooled independent experiments in wild type (n=78) versus *rde-4(ne299)* (n=100) animals. See Figure S1 for detailed description of worm schematic legend. Error bars represent SEP.